Online Appendix 12.A: Code used to generate the FROC plots

The following code, in file **MainFrocCurvePop.R**, was used to generate the population FROC curves shown in Fig. 12.2 (A - C). The values of **mu** were 0.5, 1 and 2, corresponding to the plots (A), (B) and (C) , respectively, in this figure. Using these successive values of **mu**, **source** the code 3 times, getting Fig. 12.2 (A - C). A brief explanation of the code follows, but to really understand it one has to decrease the numbers of cases, as digesting 10,000 values in one fell swoop can be hard.

Online Appendix 12.A.1: Code listing

```
# MainFrocCurvePop.R
rm(list = ls())
library(RJafroc)

seed <- 1;set.seed(seed)
mu <- 0.5;lambda <- 1;nu <- 1 ;zeta1 <- -Inf;K1 <- 10000;K2 <- 10000
#K1 <- 4;K2 <- 3
Lmax <- 2;Lk2 <- floor(runif(K2, 1, Lmax + 1))

frocDataRaw <- SimulateFrocData(
  mu = mu, lambda = lambda, nu = nu,
  K1 = K1, K2 = K2, Lk2 = Lk2, zeta1 = zeta1
)

plotFROC <- PlotEmpiricaOperatingCharacteristics(dataset = frocDataRaw, trts= 1, rdrs = 1,
opChType = "FROC", lgdPos = "NULL")
print(plotFROC$FROCPlot)
```

The **RJafroc** package is loaded at line 3. It contains the function **SimulateFrocData()** which, as the name suggests, simulates FROC data based on the Radiological Search Model (RSM). It also contains the function **PlotEmpiricaOperatingCharacteristics()**, which generates empirical plots. It returns a **ggplot2** object and the next line "**print**s" it, i.e., displays it in the **Plots** window. Several plots are possible with FROC data, deferred to **Chapter 13**, but in this code only its ability to generate FROC plots is used by setting, at line 15, the operating characteristic type option **opChType** to **"FROC"**. Line 6 initializes the parameters of the simulator: **mu** is the perceptual SNR; **lambda** is the intrinsic propensity of the observer to find suspicious regions that are non-diseased, and therefore potential NL marks (the actual number of NL marks per case is determined by a combination of **mu**, **lambda**, **zeta1**, and Poisson sampling, decreasing to zero NLs per case as **mu** is increased to infinity). Do not expect to understand it completely at this stage. The parameter **nu** is the intrinsic ability of the observer to find lesions and therefore potential LL marks (the actual number of LL marks per case is determined by a combination of **mu**, **nu**, **zeta1**, and binomial sampling, increasing to the number of lesions in the case as **mu** or **nu** is increased to infinity. Again, do not expect to understand it completely at this stage. **Lmax** is the maximum number of lesions per case in the dataset. It has been set to 2; so diseased cases are constrained to contain at most 2 lesions (the actual number of lesions per diseased case is determined by line 8). **zeta1** is the threshold parameter determining whether a suspicious region is marked. It has been set to **-Inf**, so every suspicious region is marked, no matter how low its degree of suspicion. As usual, **K1** and **K2** are the numbers of non-diseased and diseased cases respectively.

Online Appendix 12.A.2: Explanation using fewer cases

Since listing 10,000 values is not conducive to understanding what is going on, temporarily set **K1 <- 4** and **K2 <- 3** (uncomment line 7) and ensure that mu **<- 1**. Click on **Source**: this yields Fig. 12.A.1, the "raw" FROC curve.

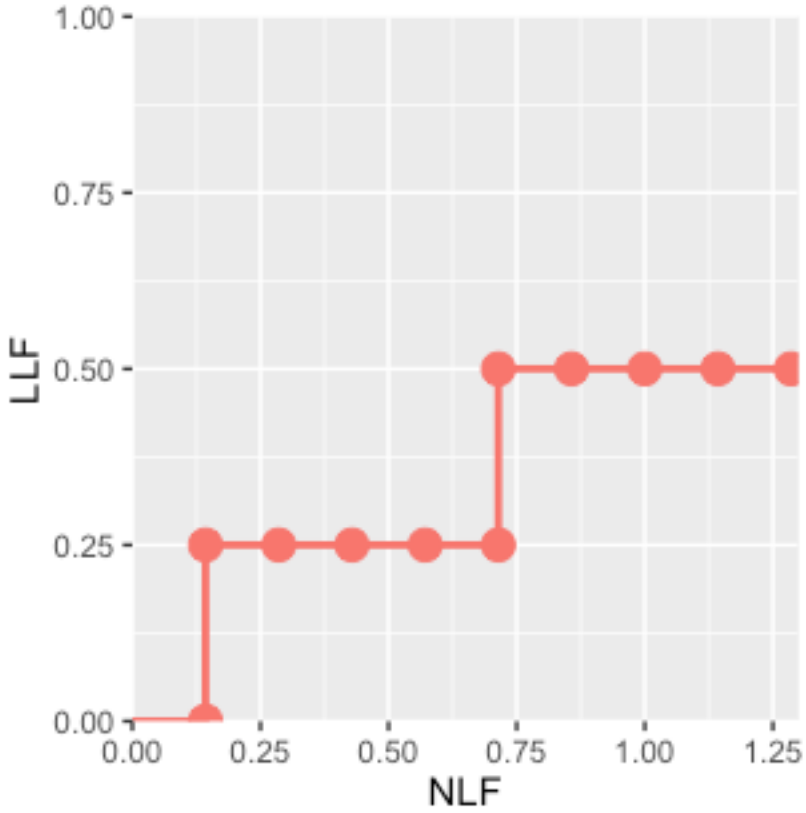

Fig. 12.A.1: Raw FROC curve produced by 4 non-diseased and 3 diseased cases. Note the 9 rightward jumps and the two upward jumps, explained below.

It consists of 9 rightward jumps, ending at $NLF_{\max} = 9/7 = 1.29$, and two upward jumps, ending at $LLF_{\max} = 2/4 = 0.5$. Highlight **Lk2** (the array containing the number of lesions per diseased case) and click **Run**.

Online Appendix 12.A.3: Code Snippet

```
> Lk2
[1] 1 1 2
```

This tells us that the first two diseased cases contain one lesion each, and the 3rd and last diseased case contains 2 lesions. (These numbers were randomly generated, subject to the constraint that the maximum number of cases is **Lmax <-** 2, by line 8 in the main file.) Altogether there are 4 lesions, and it is highly unlikely that any two of them will yield identical z-samples, one expects at most 4 upward jumps for the raw curve due to LL z-samples exceeding **zeta1**. There are actually only two. To examine what is going on, examine the structure of **frocDataRaw**, using our old friend the **str()** function.

Online Appendix 12.A.4: Code Snippet

```
> str(frocDataRaw)
List of 8
 $ NL          : num [1, 1, 1:7, 1:3] 0.487 -Inf 0.738 1.512 -0.621 ...
 $ LL          : num [1, 1, 1:3, 1:2] -Inf 0.955 0.108 -Inf -Inf ...
 $ lesionNum   : num [1:3] 1 1 2
 $ lesionID    : num [1:3, 1:2] 1 1 1 -Inf -Inf ...
 $ lesionWeight: num [1:3, 1:2] 1 1 0.5 -Inf -Inf ...
 $ dataType    : chr "FROC"
 $ modalityID  : chr "1"
 $ readerID    : chr "1"
```

The list members one is interested in are NL and LL. To view them, use the following code:

Online Appendix 12.A.5: Code snippet

```
> frocDataRaw$NL[1,1,,]
          [,1]       [,2]       [,3]
[1,]  0.4874291 -0.8204684       -Inf
[2,]       -Inf       -Inf       -Inf
[3,]  0.7383247  0.5757814       -Inf
[4,]  1.5117812  0.3898432 -0.3053884
[5,] -0.6212406       -Inf       -Inf
[6,] -2.2146999       -Inf       -Inf
[7,]       -Inf       -Inf       -Inf
> frocDataRaw$LL[1,1,,]
         [,1] [,2]
[1,]     -Inf -Inf
[2,] 0.9550664 -Inf
[3,] 0.1080789 -Inf
```

The cases are counted as follows. Since each case can contribute NLs, there are a total of 7 cases listed as a consequence of executing **`frocDataRaw$NL[1,1,,]`**. The first 4 lines correspond to non-diseased cases and the following three lines correspond to the diseased cases. In contrast, there are a total of 3 cases listed as a consequence of executing **`frocDataRaw$LL[1,1,,]`**. These are the diseased case LL ratings. Obviously LLs are impossible on non-diseased cases.

Counting the number of LLs ratings that are not **`-Inf`**, one gets 2 (the corresponding ratings are 0.955 and 0.108). These account for 2 vertical upward jumps in Fig. 12.A.1. Counting the number of NLs that are not **`-Inf`**, one gets 9. These account for 9 horizontal rightward jumps in the figure.

So what is going on? Why did 4 lesions give only 2 LL marks? This is because 2 of the four lesions were not found: one in the 1st diseased case (the two **`-Inf`** values mean that the solitary lesion on this case was not found) and one in the 3rd diseased case (the single **`-Inf`** value means that only one of the two lesions on this case was found). Examining the NL values in Appendix 12.A.5, one sees that the 1st non-diseased case generated 2 NLs, the 2nd did not generate any (a perfect decision!), the 3rd generated 2, the 4th generated 3 (a particularly troublesome case), the 5th (i.e., the 1st diseased case) generated one, the 6th (i.e., the 2nd diseased case) generated one, and the 7th (i.e., the 3rd diseased case) generated none (this case, which has two lesions, generated one LL, the other lesion was missed and no NLs were generated – altogether a mixed bag).

This should give you a feel for the structure of the data and how NLs and LLs determine the raw FROC curve. The data structure is more complicated than ROC because the number of NLs and LLs are both (integer, non-negative) random variables and NLs are possible on both non-diseased and diseased cases. That is the reason why the NL array is of length 7 in the 3rd dimension (the first two dimensions correspond to modality and reader, one each in this example). The 4th dimension indexes the NL marks on any given case.

The following code, in file **`MainFrocCurveBinned.R`**, was used to generate in Fig. 12.2 (D - F). The values of **`mu`** were 0.5, 1 and 2, corresponding to the plots (D), (E) and (F) in the figure.

Online Appendix 12.A.6: Code listing

```
# mainFrocCurveBinned.R
rm(list = ls())
library(RJafroc)

seed <- 1;set.seed(seed)
mu <- 0.5;lambda <- 1;nu <- 1 ;zeta1 <- -1;K1 <- 50;K2 <- 70; nBins <- 5
Lmax <- 2;Lk2 <- floor(runif(K2, 1, Lmax + 1))

frocDataRaw  <- FROCSimulator (mu, lambda, nu, K1, K2, Lk2, zeta1 = zeta1)
frocDataBinned <- BinDataset(frocDataRaw,desiredNumBins = nBins)

plotFROC <- EmpiricalOpCharac(frocDataBinned, trts= 1, rdrs = 1, opChType = "FROC", lgdPos =
"NULL")
```

```
print(plotFROC$FROCPlot)
```

This is similar to 12.A.1 except for the additional line 10, which bins the raw data using **`BinDataset()`** and returns a binned dataset. At line 6 the number of bins **`nBins`** has been set to 5, yielding 5 operating points. Also the number of cases has been reduced to 50 non-diseased and 70 diseased. Binning a huge number of cases is time consuming and not instructive; if the number of cases is too small, then the binning program may not be able to find the desired number of bins, and the plot may have fewer operating point. The reader should modify the number of cases to thoroughly understand these statements.

Online Appendix 12.B: CAMPI and cross correlation

The author used the cross-correlation (CC), defined below, to perform *computerized analysis of mammography phantom images* (CAMPI)[1-7]. The phantom, an image of which is shown in Fig. 12.A.2, was a 4.5 cm thick uniform Lucite block containing a thin removable wax insert containing "lesion-like" objects. An image of the phantom with the insert included is termed a *test* image, Fig. 12.A.2. Because of the presence of the thick Lucite block, the contrast in this image is relatively low, i.e., the objects are relatively hard to see. We were interested in quantifying the image quality of a particular lesion in this image, for example the one pointed to by the arrow in Fig. 12.A.2.

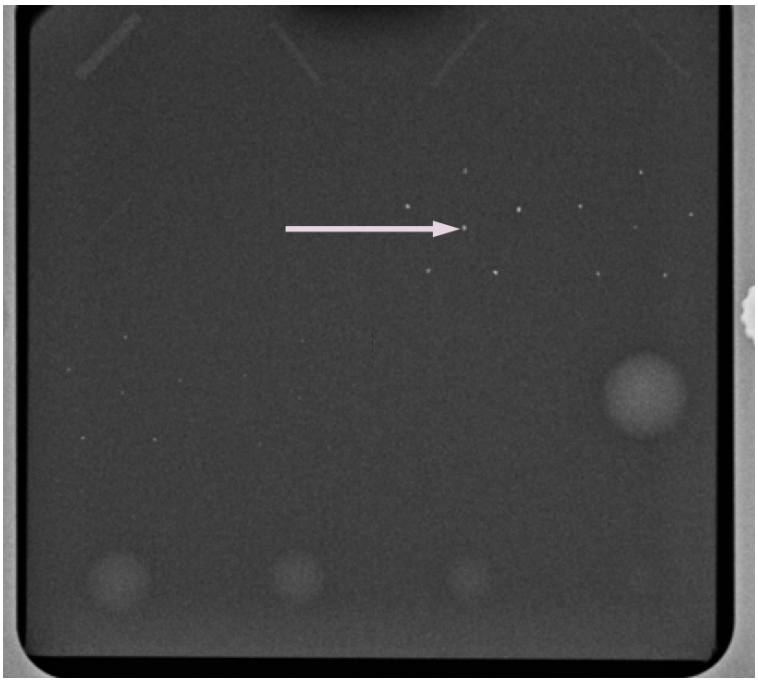

Fig. 12.A.2: Image of an American College of Radiology mammography accreditation phantom. This is the test image (wax insert inside the Lucite block) whose image quality is desired. The arrow points to a single speck whose physical SNR is to be determined.

To do this we need to know the true profile (or shape) of the lesion. The relatively thin insert can be separately imaged under high contrast conditions. Shown in Fig. 12.A.3 is the pixel value profile centered on a small calcification-like lesion, pointed to by the arrow in Fig. 12.A.2, but in the insert image[5]. Because of increased x-ray attenuation, the pixel values are smaller inside the calcification than outside it. Fig. 12.A.3 is the expected lesion profile of the template, whose pixel value is defined as $PV_{temp}(i,j)$. Because of pixelation, i and j take on integer values from 1 to I and 1 to J respectively, where for this small lesion, $I = J = 31$ was enough to encompass the simulated lesion. Define $PV_{test}(x,y)$ as the pixel value at (integer) location x, y of the test image, Fig. 12.A.3.

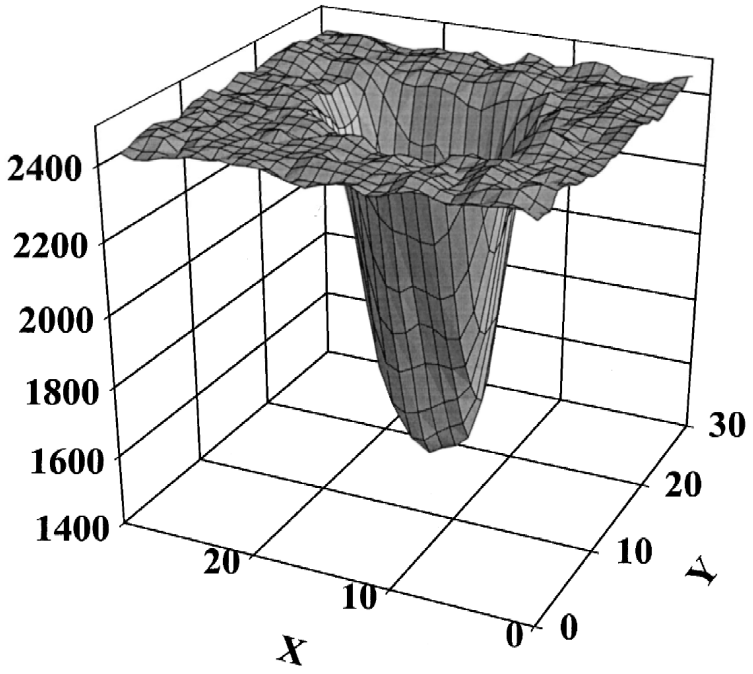

Fig. 12.A.3: This figure shows the gray scale values for the central speck of the largest microcalcification group for an insert image. This image of the phantom wax insert only was obtained at 22 kVp and under low scatter conditions. Ten insert images were obtained. The figure shows the result of aligning and averaging 10 profiles. In all 12 profiles like this corresponding to the different specks made up the microcalcification templates for this phantom.

The cross correlation $CC(x,y)$ is defined by ($\langle PV_{temp} \rangle$ is the average value of the template)

$$CC(x,y) = \sum_{j=1}^{j=J} \sum_{i=1}^{i=I} PV_{test}(x+i, y+j) \left[PV_{temp}(i,j) - \langle PV_{temp} \rangle \right] \qquad \textbf{(12.1.1)}$$

Defining (S = signal, N =noise)

$$CC_s = CC(x,y)\big|_{(at\ lesion\ location)}$$
$$CC_n = CC(x,y)\big|_{(at\ lesion free\ location)} \qquad \textbf{(12.1.2)}$$

SNR is defined by

$$SNR = \frac{CC_s - mean(CC_n)}{std(CC_n)} \qquad \textbf{(12.1.3)}$$

In other words, one calculates the cross-correlation with the template centered on the test image at the lesion location, subtracts the mean of similar measurements made at lesion-free locations, yielding the numerator of SNR. The denominator is the standard deviation of the cross-correlation measurements made at lesion-free locations on the test image. The SNR defined this way is termed, in model observer terminology, as the zero-suppressed non-pre-whitening matched filter[8-12].

Online Appendix 12.C: The Bunch transforms

This appendix is for those who wish to understand the Bunch et al paper in more depth. This paper has certain transformations, sometimes referred to as the *Bunch transforms*, which relate an ROC plot to an FROC plot and vise-versa. *It is not a model of FROC data*. It is of historical interest, and one of the reasons for including it is because this relatively obscure paper is so overlooked, if the author does not write it, no one else will.

Online Appendix 12.C.1: The Bunch transforms and the Poisson assumption

Bunch et al addressed the problem of predicting an ROC plot from a FROC plot and vice-versa. The coordinates of an ROC plot are (*FPF*, *TPF*) while those of an FROC plot are (*NLF*, *LLF*). The ROC plot is parameterized by a threshold variable ζ, which varies from positive infinity to negative infinity as one "climbs up" the ROC plot (Chapter xx). In the Bunch et al model the number of NLs per case (what we are calling *NLF*) is assumed to follow a Poisson distribution with mean λ_ζ, where this parameter obviously depends on the choice of reporting threshold (as will be shown below, ζ is the threshold parameterizing the FROC-predicted ROC plot; *we emphasize that* ζ *is an ROC threshold that applies to the whole case, not specific locations in the case*). By the Poisson assumption, the probability mass function (the discrete analog of a probability density function) of observing a case with n_1 NLs at or above confidence level ζ, is given by:

$$P\left(n_1 \mid \lambda_\zeta\right) = \mathrm{e}^{-\lambda_\zeta} \frac{\lambda_\zeta^{n_1}}{n_1!} \qquad \textbf{(12.1.4)}$$

Since λ_ζ is the mean number of NLs per case, it is estimated by *NLF*.

$$\widehat{\lambda_\zeta} = NLF_\zeta \qquad \textbf{(12.1.5)}$$

The Bunch et al model does not involve comparing the observer's threshold to the decision variable associated with each NL location - indeed, it does not characterize each NL with a *local* decision variable. Rather, as the ROC reporting threshold ζ is lowered, λ_ζ increases according to the relation $\lambda_\zeta = -\ln\left(\Phi\left(\zeta\right)\right)$, derived below, Eqn. xx. As the observer lowers the ROC confidence level ζ, $\Phi\left(\zeta\right)$ decreases, since $\Phi\left(\zeta\right) \le 1$, λ_ζ increases. This means *NLF* increases and the observer marks the additional NL locations that "pop-up" randomly following the Poisson process, i.e., one cannot say exactly which case will have how many additional NL counts, only that on the average the cases will have more NL counts.

Online Appendix 12.C.2: The Bunch transforms: x-coordinates

The probability of observing a case with a false positive at or above a given confidence level is the complement of the probability of observing a case with zero NLs:

$$P\left(FP\right) = 1 - \mathrm{e}^{-\lambda_\zeta} \qquad \textbf{(12.1.6)}$$

Now, $P\left(FP\right)$ is estimated by *FPF*:

$$\widehat{P\left(FP\right)} = FPF \qquad \textbf{(12.1.7)}$$

Since λ_ζ is estimated by *NLF*[1], it follows that:

$$FPF(\zeta) = 1 - e^{-NLF(\zeta)} \quad \textbf{(12.1.8)}$$

This equation relates the FROC abscissa to the ROC abscissa. To go the other way we use:

$$NLF(\zeta) = -\ln(1 - FPF(\zeta)) \quad \textbf{(12.1.9)}$$

In the binormal model (Chapter 06, Eqn. 6.12 and 6.13):

$$1 - FPF(\zeta) = \Phi(\zeta) \quad \textbf{(12.1.10)}$$

Therefore, the mysterious inverse relation between λ_ζ and ζ, alluded to previously, is:

$$\lambda_\zeta = -\ln(\Phi(\zeta)) \quad \textbf{(12.1.11)}$$

As the ROC threshold parameter λ_ζ increases $\Phi(\zeta) \to 1$ and $\lambda_\zeta \to 0$. Conversely, as the ROC threshold parameter ζ decreases $\Phi(\zeta) \to 0$ and $\lambda_\zeta \to \infty$. Swensson also derived Eqn. xx in his extension of the LROC model to predict FROC data[13].

Online Appendix 12.C.3: The Bunch transforms: y-coordinates

To relate the FROC quantities to the ROC ordinate, note that a FN event (the complement of a TP event) requires the *simultaneous* occurrence of two events: the lesion must be missed, the probability of which is 1-*LLF*[2], and no non-lesions are marked, the probability of which is $e^{-\lambda_\zeta}$. Therefore, assuming independence of the two events, the ROC ordinate, *TPF*, is given by:

$$1 - TPF = (1 - LLF)e^{-\lambda_\zeta} \quad \textbf{(12.1.12)}$$

Estimating λ_ζ by *NLF* and using Eqn. xx, we get

$$1 - TPF = (1 - LLF)(1 - FPF) \quad \textbf{(12.1.13)}$$

Solving this equation for *LLF* yields

$$LLF = (TPF - FPF)/(1 - FPF) \quad \textbf{(12.1.14)}$$

As with the NLs, *the Bunch et al model does not involve comparing the observer's threshold to the decision variable associated with each LL location* (indeed, it does not characterize each LL with a decision variable).

[1] This involves an independence assumption that the distribution of NLs is unaffected by the presence of lesions, if any.

[2] This assumes one lesion on every diseased case. In their paper Bunch et al extend it to multiple lesions per diseased case.

Rather, the right hand side of Eqn. xx predicts *LLF* from the ROC plot, and this multiplied by the total number of lesions gives the number of lesions that "pop-up" and the observer is assumed to mark all of these lesions.

The following table summarizes the Bunch transformations. It is understood that all variables are functions of the ROC reporting threshold ζ.

Table 12.1: The Bunch et al transformations

Direction of transformations	Ordinate	Abscissa
ROC → FROC	$LLF = (TPF - FPF)/(1 - FPF)$	$NLF = -\ln(1 - FPF)$
FROC → ROC	$TPF = 1 - (1 - LLF)e^{-NLF}$	$FPF = 1 - \mathrm{e}^{-NLF}$

Online Appendix 12.C.4: Discussion of the Bunch transforms

The Bunch transforms do not specify the shape of the FROC plot. That would require a model for the free-response mark-rating pairs. Rather, if one has a model for ROC data, and we have covered several in previous chapters, then it allows the ROC plots to be mapped to FROC plots. Conversely, if one has a model for the FROC plot, it allows the FROC plot to be mapped to a ROC plot. Since a model for FROC data has not been described yet, it appears in a later chapter, let us pursue the first approach and see where this takes us. The binormal model predicted ROC plot is:

$$FPF(\zeta) = \Phi(-\zeta)$$
$$TPF(\zeta) = \Phi(a - b\zeta) \qquad \textbf{(12.1.15)}$$

The ROC data used is that in Table 4.1 in **Chapter 04**. This was analyzed in **Chapter 06**, where the binormal model *a*, *b* parameters were found to be 1.3204 and 0.6075, respectively. Here is the code (in file **`MainBunchTransforms.R`**) to calculate the ROC plot and convert it to an FROC plot.

```
rm(list=ls())
a <- 1.3204 # see Univariate binormal model, Eqn. xx
b <- 0.6075
mu <- a/b; sigma <- 1/b
zeta = seq(-2,mu+3, 0.1)
FPF <- pnorm(-zeta)
TPF <- pnorm(a-b*zeta)
plot(FPF, TPF, type = "l", xlim=c(0,1), ylim=c(0,1))
LLF <- (TPF-FPF)/(1-FPF)
NLF <- -log(1-FPF)
plot(NLF, LLF, type = "l", xlim=c(0,max(NLF)), ylim=c(0,1))
```

The logic of this code should, by now, be fairly obvious to you. The **`xlim`** and **`ylim`** arguments to the **`plot`** functions simply supply the plotted ranges. **`Sourcing`** this code gives the following plots, Fig. 12.A.4, where the left panel is the ROC plot and the right panel is the predicted FROC plot.

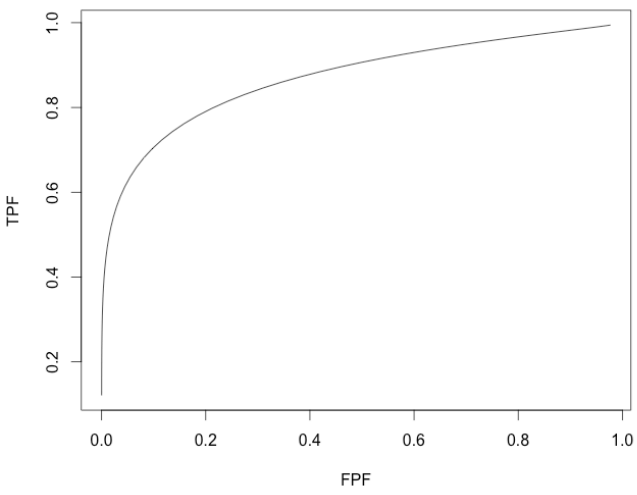

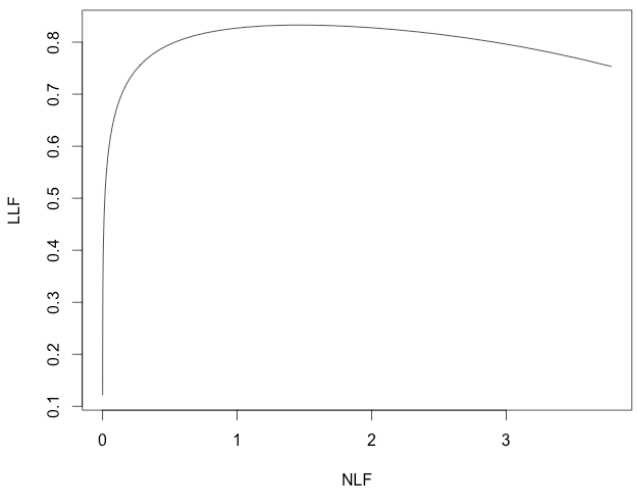

Fig. 12.A.4: TBA

Clearly something is wrong with the predicted FROC plot: one expects it to plateau, not bend over and head downwards, as in the right panel of Fig. 12.A.4. This would imply that as the confidence level is lowered the observer *unmarks* some of the lesions that were previously marked at a *higher* confidence level. Dr. James Sorenson (co-author of a notable textbook on nuclear medicine physics[14]) tried to analyze FROC data using the above transformations (private communication, ca. 1988) but the problem he encountered was that a binormal fitted ROC plot generally crosses the chance diagonal near the upper right corner, see Chapter xx. When this happens *TPF* = *FPF* and the predicted *LLF* is zero (the observer unmarks all previously marked lesions!). Worse, the binormal fitted plot has a "hook" where *FPF* > *TPF*. When that happens *the predicted LLF is negative* (since there is nothing to unmark, this is clearly impossible). The author acknowledges that Jim communicating his thoughts set in motion some thoughts of his own which led to the publication of the maximum likelihood method for fitting FROC plots[15,16] and the author's continued interest in this field.

On the other hand, if one had a model for the FROC plot, the Bunch transforms predict a proper ROC plot. Repeating the second row of Table 12.1:

$$TPF = 1 - (1 - LLF)e^{-NLF} \qquad \textbf{(12.1.16)}$$

$$FPF = 1 - \mathrm{e}^{-NLF} \qquad \textbf{(12.1.17)}$$

Since $1 - LLF \le 1$, multiplying it into e^{-NLF} and subtracting from one yields a *larger* number than 1-e^{-NLF}, in other words, the above equations *guarantee* that *TPF* is always greater than or equal to *FPF*, so the ROC plot can never cross the chance diagonal, so it must be proper. The problem was with the ROC curve fitting procedure. If Dr. Sorenson had access to a proper ROC curve fitting procedure (which maintains $TPF \ge FPF$) he would not have encountered the problem demonstrated in Fig. 12.A.4. Unfortunately, this was before the proper ROC curve fitting procedure was invented[17].

There is a tendency among medical physicists to assume that just because the lesion is in the image, the observer can find it, if only they used a detailed raster-scan mode of examining the image. This misconception is also prevalent in the computer aided detection (CAD) community, where it is assumed that CAD has perfect search-performance (because it "looks" at everything: Dr. Ronald Summers MD, private communication,

Medical Image Perception Society meeting, 9–12 August 2011, Dublin, Ireland), when in fact CAD is very poor at search compared to expert radiologists.

References

1. Chakraborty DP, Sivarudrappa M, Roehrig H. Computerized measurement of mammographic display image quality. Paper presented at: Proc SPIE Medical Imaging 1999: Physics of Medical Imaging1999; San Diego, CA.
2. Chakraborty DP, Fatouros PP. Application of computer analyis of mammography phantom images (CAMPI) methodology to the comparison of two digital biopsy machines. Paper presented at: Proc SPIE Medical Imaging 1998: Physics of Medical Imaging; 24 July 1998, 1998.
3. Chakraborty DP. Comparison of computer analysis of mammography phantom images (CAMPI) with perceived image quality of phantom targets in the ACR phantom. Paper presented at: Proc. SPIE Medical Imaging 1997: Image Perception; 26-27 February 1997, 1997; Newport Beach, CA.
4. Chakraborty DP. Computer analysis of mammography phantom images (CAMPI). *Proc SPIE Medical Imaging 1997: Physics of Medical Imaging.* 1997;3032:292-299.
5. Chakraborty DP. Computer analysis of mammography phantom images (CAMPI): An application to the measurement of microcalcification image quality of directly acquired digital images. *Medical Physics.* 1997;24(8):1269-1277.
6. Chakraborty DP. The Effect of the Anti-Scatter Grid and Target/Filters in Full-field Digital Mammography. Paper presented at: Proc. SPIE Medical Imaging 1999: Physics of Medical Imaging1999.
7. Chakraborty DP. The Effect of the Anti-Scatter Grid on Full-Field Digital Mammography Phantom Images. *Journal of Digital Imaging.* 1999;12(1):12-22.
8. Tapiovaara MJ. Objective Measurement of Image Quality in Fluoroscopic X-ray Equipment: Fluoroquality. *STUK-A196.* 2003.
9. Tapiovaara MJ, Wagner RF. SNR and noise measurements for medical imaging: I. A practical approach based on statistical decision theory. *Phys Med Biol.* 1993;38:71-92.
10. Tapiovaara MJ. SNR and noise measurements for medical imaging: II. Application to fluoroscopic x-ray equipment. *Phys Med Biol.* 1993;38:1761-1788.
11. Eckstein MP, Abbey CK, Bochud FO. A Practical Guide to Model Observers for Visual Detection in Synthetic and Natural Noisy Images. In: Kundel H, Beutel J, Van-Metter R, eds. *Handbook of Medical Imaging*. Bellingham, Washington: SPIE; 2000:593-628.
12. Chakraborty DP. An alternate method for using a visual discrimination model (VDM) to optimize softcopy display image quality. *Journal of the Society for Information Display.* 2006;14(10):921-926.
13. Swensson RG. Unified measurement of observer performance in detecting and localizing target objects on images. *Med Phys.* 1996;23(10):1709 -1725.
14. Cherry SR, Sorenson JA, Phelps ME. *Physics in Nuclear Medicine.* 4th ed. Orlando: Elsevier, Saunders; 2012.
15. Chakraborty DP. Maximum Likelihood analysis of free-response receiver operating characteristic (FROC) data. *Med Phys.* 1989;16(4):561-568.
16. Chakraborty DP, Winter LHL. Free-Response Methodology: Alternate Analysis and a New Observer-Performance Experiment. *Radiology.* 1990;174:873-881.
17. Roe CA, Metz CE. Dorfman-Berbaum-Metz Method for Statistical Analysis of Multireader, Multimodality Receiver Operating Characteristic Data: Validation with Computer Simulation. *Acad Radiol.* 1997;4:298-303.